Journal of the European Ceramic Society 43 (2023) 4877–4884

Contents lists available at ScienceDirect

Journal of the European Ceramic Society

journal homepage: www.elsevier.com/locate/jeurceramsoc

Flexible interconnected ceramic parts 3D printed by two-component material extrusion with water-soluble support structures

René Wick-Joliat *, Dirk Penner

IMPE Institute of Materials and Process Engineering, ZHAW Zürcher Hochschule für Angewandte Wissenschaften, Technikumstrasse 9, 8401 Winterthur, Switzerland

ARTICLE INFO

Keywords:
Ceramic 3D printing
Material extrusion
Support material
NaCl
Multi-material

ABSTRACT

Material extrusion (MEX) of complex thermoplastic structures often depends on the reliable printing of a water-soluble support structure. The material of choice is typically polyvinyl alcohol (PVA), which is not used in ceramic MEX printing due to a limited printing compatibility with most ceramic feedstocks (poor layer adhesion). Herein, a new thermoplastic feedstock was developed as temporary support material on the basis of NaCl mixed with a commercial injection molding binder system. The NaCl feedstock is fully compatible for MEX printing with ceramic feedstocks and showed excellent printing properties and high green body strength. The support structure is mostly dissolved in water and the rest can be removed manually or during thermal debinding. The NaCl support material was used to print flexible Al_2O_3 samples with hinges or chainmail samples. This strategy is an attractive way to introduce additional functionality and new applications which were so far inaccessible to technical ceramics.

1. Introduction

Material extrusion (MEX, also called FFF or FDM) is an established 3D printing method for thermoplastics and was adopted for ceramics by filling a thermoplastic binder with high volumes of a ceramic powder (>40 vol%). This ceramic feedstock can be 3D printed and then the binder is removed from the printed part (in a solvent bath and/or thermally) and the part is finally densified by sintering.

In MEX printers, the material is fed into the extrusion unit either as filament or as a granulate. The advantage of using filaments is a slightly higher printing quality since the material extrusion can be steered accurately by pushing forward or retracting the filament. However, filament fabrication from highly filled ceramic feedstocks is delicate and requires special effort to reduce brittleness and improve the flexibility while avoiding buckling and clogging of the nozzle. The development of granulated feedstocks is more straightforward and the requirements for a granulated MEX printing feedstock overlap with the requirements for ceramic injection molding (CIM) feedstocks. Consequently, most CIM feedstocks are suitable for granulate MEX printing without or with minor modifications [1,2]. This approach is attractive for several reasons. Firstly, CIM feedstocks are cheap and readily available. Furthermore, optimized debinding and sintering conditions are well known, and only minor adjustments are necessary depending on the geometry of the printed parts. Finally, the same material can be used for prototyping by 3D printing that is employed later in mass-production by CIM.

Numerous groups have studied MEX printing on a wide range of ceramic materials including but not limited to Al_2O_3 [3–5], ZrO_2 [1,6–9] and tricalcium phosphate [10].

Multi-material ceramic 3D printing was reported mainly for lithography-based processes [11] and material jetting [12,13]. Recently, we have described multi-material ceramic MEX printing on a self-constructed granulate-fed printer [2].

MEX printing of complex thermoplastic parts often relies on the printing of temporary support structures which enable overhangs and bridges. The support can be printed from the same material as the actual model, sometimes leading to tedious manual removal of the support and inferior surface quality. A more attractive and widely used alternative is the printing of temporary support structures from a water-soluble material such as polyvinyl alcohol (PVA) and subsequent removal of the support by dissolution an a water bath [14].

For ceramic MEX printing, however, we found that PVA is not compatible with most ceramic feedstocks due to poor adhesion between the different materials. Especially, PVA adhesion on already printed ceramic layers was insufficient and led to failed prints. Furthermore, a printing temperature of 215–230 °C is recommended for commercial PVA filaments, well above the processing and even decomposition

* Corresponding author.
E-mail address: rene.wick@zhaw.ch (R. Wick-Joliat).

https://doi.org/10.1016/j.jeurceramsoc.2023.03.069
Received 24 October 2022; Received in revised form 19 December 2022; Accepted 31 March 2023
Available online 1 April 2023

temperature of many common CIM feedstocks including the Embemould K83 binder system used in the present work (Embemould working temperature is 130 – 150 °C, decomposition starts at 170 °C). To the best of our knowledge, there are no reports of ceramic parts printed with the help of PVA support, speculatively due to the incompatibility of PVA with most ceramic feedstocks.

Herein, we present a strategy to quickly produce a fully compatible support material for ceramic MEX printing by using the same binder system but replacing the ceramic powder by readily water-soluble NaCl powder.

In this way, a support material based on the commercial CIM binder Embemould K83 with a very high NaCl loading of 67 vol% was produced and showed excellent printability. After printing, the 67 vol% of NaCl as well as approximately half of the Embemould binder were dissolved in a water bath, leaving behind a very porous and brittle support structure which could then be removed manually or thermally without remnant. The adhesion between the NaCl and ceramic feedstock was excellent and complex Al_2O_3 parts were successfully printed, debound and sintered. For example, different movable hinges, chains and multi-gear systems were fabricated. Furthermore, a series of meshes or chain-mail structures was designed, inspired by the work of Wang et al. on the mechanical properties of 3D printed structured fabric [15] as well as ceramic artist C. Kempernik who specialized on interconnecting clay rings into chains and meshes [16].

The addition of those functionalities to technical ceramics could make new applications such as fully ceramic conveyor belts for high temperature applications, ceramic fabrics or jewelry (3D printed ceramic bracelets or wristbands for watches) possible. The strategy of producing fully compatible support materials from NaCl should be applicable to all CIM binder systems as well as for metallic MEX printing.

As a next step, structures printed from NaCl feedstock can also be sintered and used as water soluble molds for metal casting. This approach was demonstrated by N. Kleger et al. for direct ink writing [17] and stereolithography [18] of NaCl molds for casting of magnesium, aluminum and other materials.

2. Experimental

2.1. General

NaCl was purchased from Sigma-Aldrich (99.5%). The organic binder system, Embemould K83, as well as the Al_2O_3 ceramic injection molding feedstock (kcmold® 200063.1, 96% Al_2O_3) were supplied by Krahn Ceramics. LDPE (LD 655) was bought from ExxonMobil.

2.2. Feedstock preparation

NaCl feedstocks were prepared by grinding commercial NaCl powder in a Nutri Bullet 600 blender and removing the larger crystals (>100 μm) by sieving. Then, 80 wt% of NaCl (<100 μm) were manually mixed with 19.2 wt% Embemould K83 and 0.8 wt% LDPE pellets. Those components were processed through a twin-screw extruder (Thermo Fisher, Process11 Extruder) for six times at 130 °C to ensure good homogeneity. After each extrusion, the feedstock was crushed in a Nutri Bullet blender. The granulate fraction with particle size of 200 – 500 μm was then used for 3D printing.

For printing Al_2O_3 parts, commercial CIM feedstock kcmold 200063.1 was ground and sieved to particle size of 200 – 500 μm in a Nutri Bullet blender.

2.3. Feedstock characterization

Rheological measurements of the Embemould binder were conducted on an MCR301 rheometer (Anton-Paar, Austria) with a CTD 450 heating chamber. For the measurements, a plate-plate geometry with 25 mm diameter was used in oscillation mode. The deformation was set to 0.1%, the static force to 0.25 N and the angular frequency was swept from 0.1 to 50 rad/s. The angular frequency sweep was performed at temperatures from 80 to 180 °C in 10 °C steps and with a temperature equilibration time of 1 min

Differential scanning calorimetry (DSC) analysis of the Embemould binder was carried out on a DSC 204 F1 Phoenix instrument (Netzsch, Germany) under nitrogen atmosphere with a gas flow of 40 mL/min. Aluminum pans with pierced caps were used and the samples were heated from − 80 to 180 °C with a heating rate of 20 K/min, followed by a cooling step to − 80 °C (10 K/min) and a second heating to 180 °C with a heating rate of 20 K/min. Only the second heating step was considered for thermal analysis.

Dynamic mechanical analysis (DMA; TA Instruments, Q800, Germany) was used to determine the softening point of the feedstock by using the penetration accessory for the cantilever clamp. A penetration tip was mounted to the dynamic part of the clamp and a static force of 1 N was applied during the measurement. Feedstock samples of approximately 1 mm thickness and 5 mm in diameter were placed in the sample holder at the static part of the clamp. The setup was heated from 30 to 150 °C with a heating rate of 3 K/min and the softening point was determined as the temperature where the tip completely penetrated the feedstock sample.

Thermogravimetric analysis (TGA) was conducted on a Netzsch 449 C Jupiter instrument. The samples were weighed into an Al_2O_3 crucible and heated from 20 to 600 °C at 5 K/min under 50 mL/min air flow.

Table 1
Printing parameters for the NaCl- and Al_2O_3 feedstock.

Feedstock	NaCl	Al_2O_3
Powder	NaCl, 99% purity	Al_2O_3, 96% purity, NM 9622B
Binder	Embemould K83 + LDPE	Embemould K83
Binder content	20.0 wt%, 33.1 vol%	20.0 wt%, 46.3 vol%
Pre-heating zone	70 °C	70 °C
Main heating zone	130 °C	160 °C
Nozzle diameter	0.6 mm	0.6 mm
Layer height	0.2 mm	0.2 mm
Line width	0.72 mm	0.72 mm
Printing speed	20 mm/s	20 mm/s
Perimeter lines	2	2 or 3
Infill	60–80% (alternating −45°/+45°)	100% (alternating −45°/+45°)

2.4. 3D printing

A self-constructed 3D printer equipped with two granulate-feed extrusion units was described in more detail in a previous study [2]. In short, both extrusion units are mounted to a frame moving in z-direction, while the printing bed is moved in x- and y- direction. The print heads are fixed to a linear guide which allows the inactive head to be elevated by a few millimeters by a servomotor. The granulate is stored in a reservoir funnel. The extruder contains three temperature zones, an air-cooled zone at the granulate inlet, a pre-heating zone and the main heating zone with exchangeable nozzle. The printer is controlled by a Duet 2 wifi board and slicing was done in Simplify 3D with the Dual Extrusion Wizard tool. All parts were designed in Autodesk Fusion 360. The main printing parameters for the NaCl- as well as Al_2O_3 feedstock are summarized in Table 1.

2.5. Pre-debinding/debinding/sintering

Printed parts were debound in a stirred deionized water bath at 40 °C in order to dissolve the NaCl content of the NaCl support feedstock as well as the soluble fraction of the Embemould binder system. Depending on the wall thickness, parts were debound for two to seven days with changing the water at least once in the process. The parts were rinsed

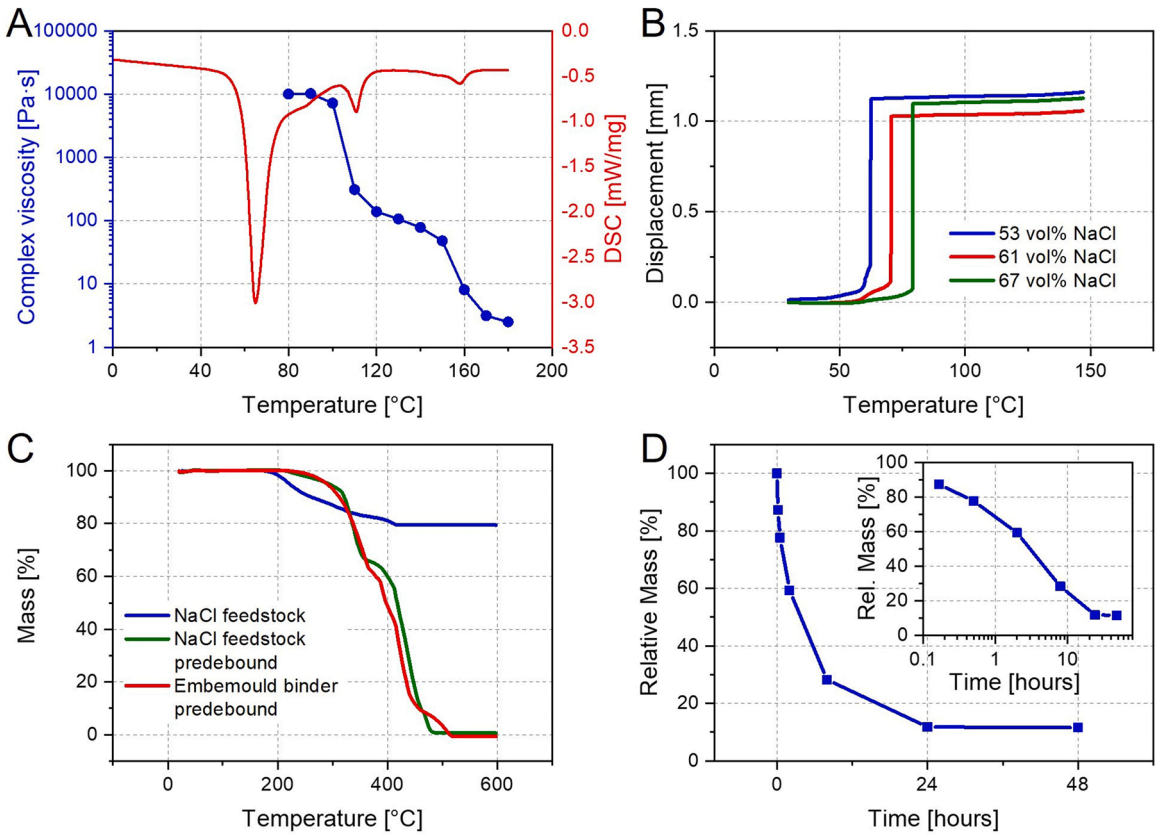

Fig. 1. A: Temperature dependent change of viscosity at 31 rad/s (oscillating mode, 0.1% deformation) and DSC of the Embemould K83 binder. B: DMA softening point tests for feedstocks with different NaCl content. C: TGA measurements of the NaCl feedstock (80 wt% NaCl) before (blue) and after (green) aqueous predebinding as well as only Embemould binder after pre-debinding (red). D: Mass loss during aqueous debinding of 3D printed sample of roughly 1 g and dimensions of 8×8×4 mm (inset: logarithmic time scale).

thoroughly with deionized water and then dried at 40 °C for at least 24 h.

After drying, the remaining support material was sometimes removed manually with a knife or spatula, but this step was not necessary, since after dissolution of the NaCl the remaining support material decomposes without remnant during thermal debinding.

Thermal debinding and sintering was performed in a Nabertherm box furnace (LHT 02/18 or LHT 04/18). Firstly, the temperature was increased to 500 °C at 50 °C/h and kept for 1 h. Then the oven was heated to the final sintering temperature of 1600 °C with 100 °C/h and a dwell time of 2 h before cooling down with 160 °C/h.

2.6. Characterization (microscopy, SEM, ICP-OES)

Light microscopy was done on a Keyence VHX 6000 and scanning electron microscopy (SEM) as well as energy-dispersive X-ray spectroscopy (EDX) on a Phenom XL Desktop SEM (Thermo Fisher Scientific).

The Na_2O content of sintered Al_2O_3 parts, which were 3D printed with and without NaCl support material, was measured by Nabaltec AG using inductively coupled plasma optical emission spectroscopy (ICP-OES) according to DIN EN ISO 11885 E22:2009–09. Samples were previously dissolved by alkaline fusion according to DIN ISO 14869–2:2003–01.

3. Results and discussion

The NaCl feedstock presented herein was prepared with a commercial CIM binder because of the similar requirements for a CIM feedstock and a ceramic MEX feedstock. In previous work, we used the Embemould K83 binder system for CIM of Al_2O_3 [19] as well as conductive $MoSi_2/Al_2O_3$/feldspar composites [20] and for multi-material MEX printing of colored ZrO_2 [2]. Utilizing the same binder system for the NaCl support feedstock ensures a high compatibility of the NaCl feedstock with the various ceramic feedstocks we developed earlier. DSC and rheology measurements show that the Embemould binder consists of at least four components with melting temperatures of 65, 87, 111 and 158 °C (Fig. 1A). The viscosity of the binder decreases by roughly one order of magnitude each time the melting point of one component is exceeded and becomes liquid above 160 °C, when all components are molten. The different melting temperatures will have important effects on the behavior of the ceramic feedstocks containing this binder system. For example, above 65 °C, the feedstocks typically soften and become

Table 2
Filament extrusion of Embemould/NaCl composite feedstock at different temperatures and different extrusion speeds. Extrusion was controlled by the Duet Web Control interface. For all experiments, extrusion amount was set to 10 revolutions of the extruder screw and extrusion speed was set as revolutions per second.

Temperature (°C)	Extrusion Speed (revolutions s^{-1})	Filament weight (g)	Standard Deviation (g)	Relative St. Dev. (%)
110	0.2	0.2026	0.0014	0.69%
	0.6	0.2033	0.0005	0.26%
	1.0	0.2026	0.0014	0.69%
130	0.2	0.2008	0.0010	0.49%
	0.6	0.2035	0.0020	0.98%
	1.0	0.2025	0.0017	0.82%
150	0.2	0.2030	0.0021	1.01%
	0.6	0.2041	0.0017	0.84%
	1.0	0.2029	0.0020	0.97%

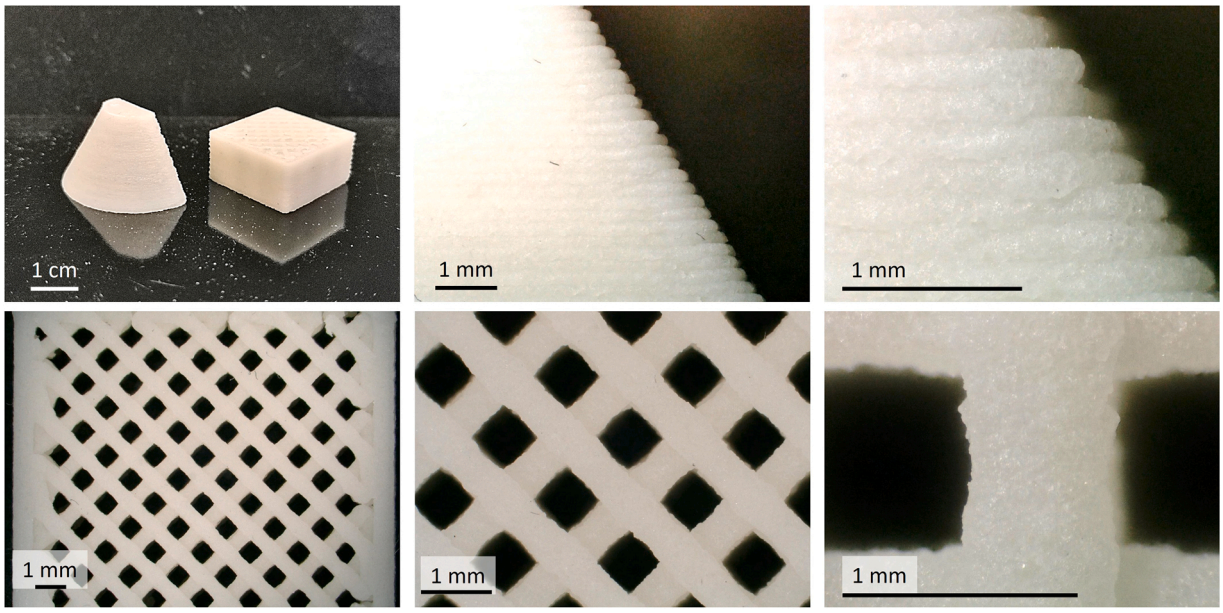

Fig. 2. Photograph and optical microscopy images of NaCl/Embemould test parts pyramid and square at different magnifications.

slightly sticky. Therefore, the heating bed of the 3D printer as well as the pre-heating zone of the extruder were set to 70–90 °C (as discussed in more detail below or in [2]).

Firstly, the NaCl content of the feedstock was optimized. Feedstocks containing 52.9 vol% of NaCl were found to leak from the extrusion nozzle even at temperatures as low as 100 °C. Increasing the NaCl content to 60.6 vol% mostly resolved this problem and a NaCl content of 66.9 vol% led to steady extrusion over a wide range of temperatures and extrusion speeds (Table 2) as well as good printing quality. A higher NaCl content also results in a higher fraction of the NaCl support structures that is dissolved after printing and therefore more porosity and easier removal of the insoluble part of the support structure.

The softening point of feedstocks with different NaCl contents was accessed by DMA. A penetration tip with a diameter of 1 mm was pressed into a sample of the feedstock of roughly 1 mm thickness and 5 mm in diameter. At a constant force on the tip, the temperature was increased until the tip penetrated the feedstock sample (Fig. 1B). The softening point of the feedstock containing 52.9 vol% of NaCl was 62 °C, close to the melting point of the first component of Embemould. By increasing the NaCl content to 66.9 vol%, the softening point increased to 78 °C.

Thermogravimetric analysis (TGA) of the NaCl feedstock with 66.9 vol% or 80 wt% NaCl before dissolution showed a mass loss of 20% at 600 °C, meaning that all the binder was decomposed and the 80 wt% NaCl remained (Fig. 1C). Therefore, after pre-debinding in water for 48 h, TGA revealed 100% decomposition, since no NaCl was left in the undissolved residue.

The rate of NaCl dissolution from NaCl/Embemould parts was determined by placing small samples (8×8×4 mm, approx. 1 g) in a water bath for different durations and weighing the samples after drying (Fig. 1D). After 24 h, 90% of the sample's mass was lost, meaning that all the NaCl (80 wt%) and roughly half of the binder has dissolved. Keeping the samples for an additional 24 h (48 h total) in the water bath did not increase the mass loss any further.

Before starting 3D printing with the newly developed NaCl feedstock, a suitable temperature and printing speed range was determined by extrusion experiments on the printer. For this purpose, the extruder screw was run for a fixed number of 10 revolutions and the mass of feedstock extruded from the nozzle was weighed. For each temperature and extrusion speed the test was repeated five times, the first value was discarded and the average of the remaining four as well as the standard deviation were calculated (Table 2). Extrusion was not possible at temperatures of 100 °C or below since the viscosity of the feedstock was too high. At temperatures of 110 – 150 °C, however, extrusion was very consistent with standard deviations in the extruded mass of 1% or below. Higher temperatures were not tested because the Embemould binder starts to decompose at 170 °C. Similarly, the extrusion speed (0.2, 0.6 or 1.0 revolutions per second were tested; a standard print speed of 20 mm/s corresponds to approximately 0.5 revolutions s^{-1}) did not influence the mass of extruded feedstock. The temperature and speed independence point to the fact that after the feedstock reaches a low enough viscosity, only the number of rotations of the extruder screw determines the extruded amount of feedstock. Consequently, two of the most important printing parameters, speed and temperature, can be changed without having to adjust other parameters such as extrusion multiplier. Therefore, the NaCl feedstock should be compatible with other feedstocks which require certain printing parameters for multi-material 3D printing.

NaCl parts were printed with a nozzle temperature of 130 °C. Feedstock extrusion was possible at temperatures as low as 110 °C, but extrusion was more reliable and consistent at temperatures above the melting point of the third binder component (111 °C). The preheating zone was set to 70 °C, slightly above the melting point of the primary binder component to soften feedstock before completely melting it in the extrusion zone. Adhesion of the printed parts to the printing bed was largely improved with bed temperatures above the melting point of the first binder component of 66 °C. After printing, when the bed was cooled to room temperature, NaCl parts automatically lost the adhesion to the build plate and could be detached without difficulty. A wide range of printing speeds of 4 – 25 mm/s led to good printing quality. Only at speeds higher than 30 mm/s the printing quality of some features like sharp corners was affected negatively. As a compromise between short printing time and high printing quality, most parts were printed with 20 mm/s.

A pyramid as well as a square with rectangular infill were used as test geometries for optimizing printing conditions (Fig. 2). Under optimized conditions, the parts showed no defects such as incomplete layer adhesion, oozing or flaws in the infill.

Since the NaCl/Embemould acts as support material it must be removable without leaving any trace in the actual part. The NaCl support structures were removed in a two-step process. Firstly, the NaCl as well as roughly 50 wt% of the Embemould binder dissolved in a water

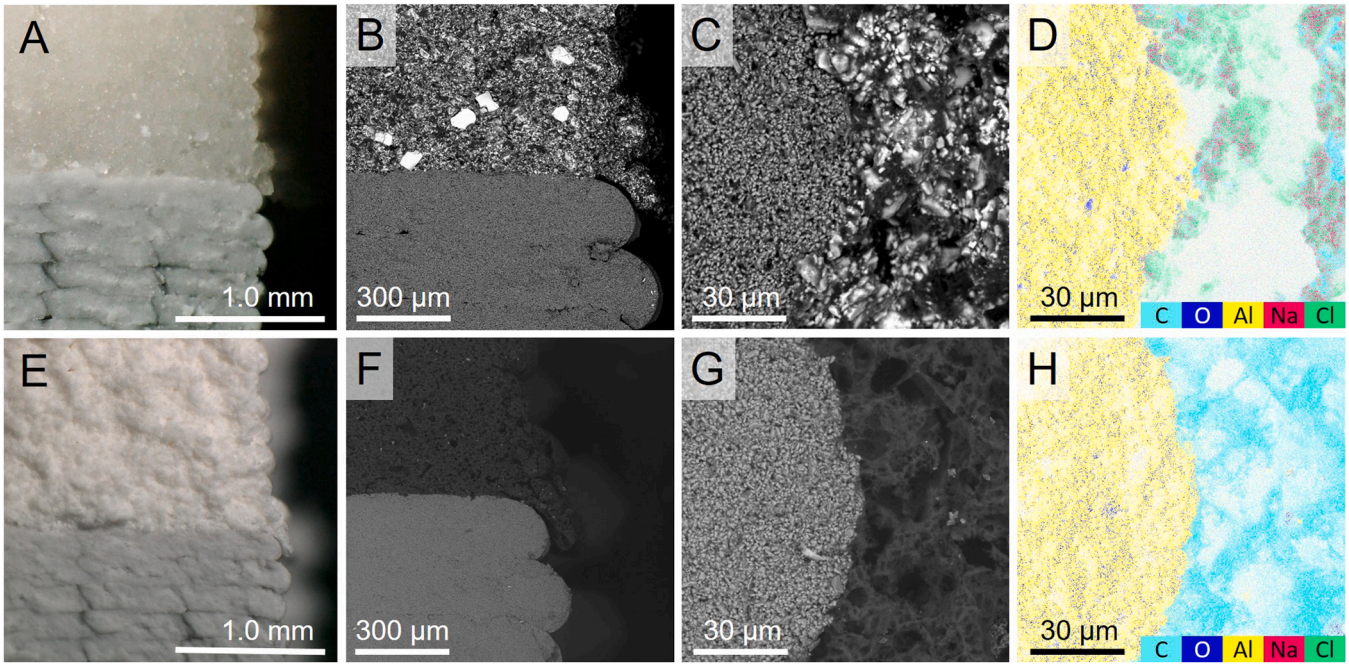

Fig. 3. A-D: Fracture analysis of a two component NaCl/Al_2O_3 part as-printed. Translucent NaCl on top, gray Al_2O_3 on the bottom. E-H: the same part after debinding and dissolution of NaCl in water. A, E: Light microscopy. B, C, F, G: SEM on an Al_2O_3/NaCl interfaces. D, H: EDX analysis showing complete removal of the NaCl.

bath at 40 °C. Dissolution times were greatly dependent on the geometry and size of the part. In small parts with wall thicknesses of < 2 mm, all NaCl was dissolved within 24 h (Fig. 1D), while larger parts and especially multi-material parts (Al_2O_3 with NaCl support) were kept in the water bath for six days with at least one water exchange after one or two days. In this first step, NaCl parts lost 90–92% of their weight and 80–85% of their volume. Without NaCl, the remaining binder was highly porous and brittle as shown by light microscopy, SEM and EDX. In the green state directly after printing, the NaCl/Embemould parts are dense and translucent. In SEM and EDX, the high loading of the binder with NaCl crystals is obvious (Fig. 3A-D). After dissolution of the NaCl, the parts lose their translucency and only a fragile network of organic binder is left (Fig. 3E-H).

The complete removal of NaCl is especially important if high purity ceramic materials are used, since even trace amounts of impurities can affect important properties such as bending strength negatively [21,22].

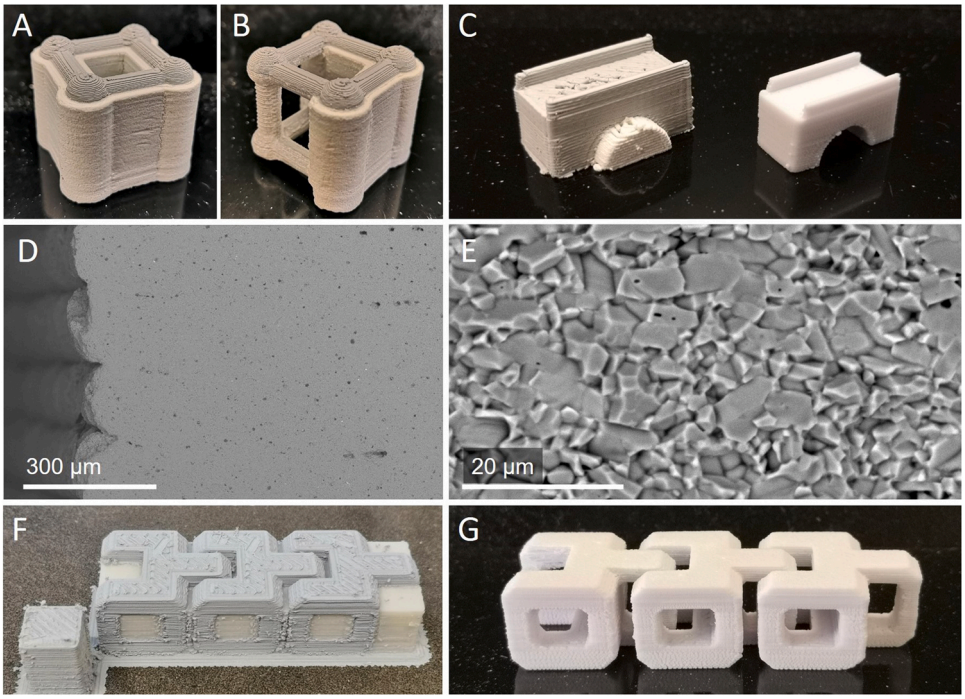

Fig. 4. A, B: Al_2O_3/NaCl parts before and after manual removal of some of the support structure. C: Al_2O_3 "bridge" in pre-debound state with the support structure and after thermal debinding and sintering. D, E: SEM image of the cross-section of a sintered 3D printed Al_2O_3 part F: Simple hinge mechanism as printed from Al_2O_3 feedstock and NaCl support feedstock. G: the same structure after sintering. The three parts are now movable.

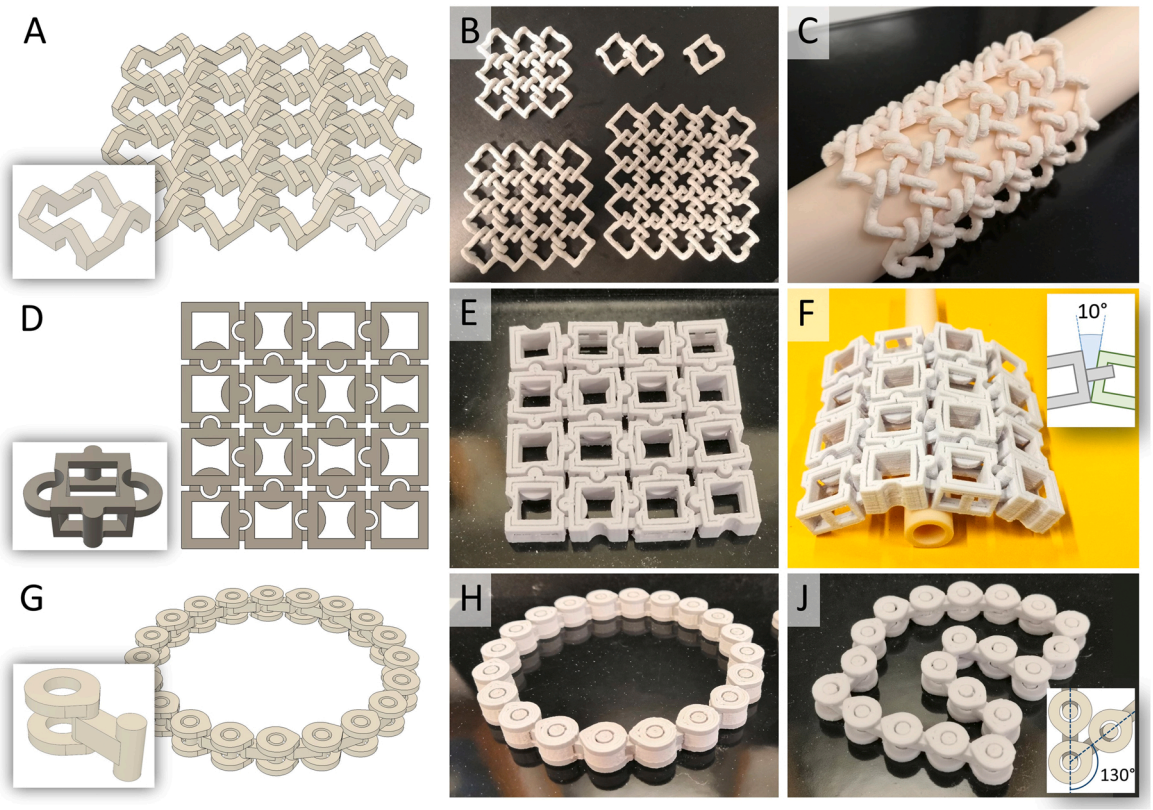

Fig. 5. A: chainmail CAD which can be printed without support structure due to overhang of max. 45°. B: Sintered Al_2O_3 meshes of different sizes from 1×1 up to 8×8 (not shown). C: Chainmail bending around a ceramic tube. D-F: Advanced chainmail design printed with NaCl support structure. G: Chain CAD design. H: Chain printed from Al_2O_3 feedstock with NaCl support. J: Fully flexible chain after sintering. Bending angle is up to 130° per chain link.

In this case, the usage of ultrapure water and multiple water changes during debinding are recommended. SEM/EDX on polished surfaces of sintered parts did not show an increased Na_2O content for samples printed with NaCl support structure and no apparent differences in microstructure were observed (details in supporting information). Furthermore, the Na_2O content as measured by ICP-OES was 0.04 wt% for all Al_2O_3 parts, independent on whether samples were printed with NaCl support or not. Since the Na_2O content is not increased, we assume that printing with NaCl support material does not negatively affect the mechanical stability of sintered ceramic parts. A detailed analysis of the mechanical properties of 3D printed ceramic parts, especially in comparison with parts injection molded from the same feedstock, is in progress but beyond the scope of the present study.

As an alternative route to avoid any sodium contamination, other highly water-soluble substance might be used instead of NaCl, e.g. sugar or ammonia salts.

After dissolution and pre-debinding in water the remaining porous support structure was removed thermally during the thermal debinding step of the ceramic parts. Since pre-debinding in water as well as thermal debinding are standard for most 3D printed ceramic parts, removal of the NaCl/Embemould support structure does not add additional steps to the ceramic process.

It is also possible to manually remove the very brittle remaining support structure with the help of a spatula or knife (Fig. 4A, B). The shrinkage and complete removal of the support structure during thermal debinding and sintering is shown in Fig. 4C. Solvent and thermal debinding of the Al_2O_3 sample result in a porous structure which then shrinks and densifies during sintering at a temperature of 1600 °C.

SEM analysis of 3D printed Al_2O_3 parts after sintering evidence the excellent layer-to-layer adhesion with very little porosity at the interfaces between layers and lines (Fig. 4D, E), which is also reflected in a high relative density of 97.5–99.7%, strongly dependent of the part geometry and the infill geometry (Supporting Table 3).

Subsequently, a simple hinge mechanism was designed connecting three individual parts into one flexible structure (Fig. 4F, G). Due to shrinkage of the ceramic parts during sintering, special care must be taken in planning the spacing between parts that should be movable in the sintered state. The horizontal spacing in between chain links or individual hinge parts was set to either 0.72 or 1.44 mm, corresponding to one or two printed lines of supporting material with a line width of 0.72 mm (standard line width for 0.6 mm nozzle). Vertically, the spacing was at least two layers of supporting material or 0.4 mm. In this way, at least one line or two layers separated the individual parts guaranteeing that were not touching even after shrinkage during sintering.

We also tested the printing and sintering of chainmail-type meshes. The first trials consisted of a square basic module, which could then be multiplied in x- and y-direction to form a two-dimensional interwoven network (Fig. 5A). The basic element had overhangs of only 45 degrees and could therefore be printed without support structure. In this way, meshes composed of up to 64 (8×8) basic squares were realized. The flexibility of the meshes can be fine-tuned by adjusting the spacing between the individual links. For example, a vertical spacing of 0.3 mm led to a very stiff mesh that could only be bent by a few degrees, while 0.5 mm of spacing gave the mesh shown in Fig. 5 that could be rolled up completely. Using this strategy, the fabrication of meshes with different flexibility in x- and y-direction is possible.

Next, a more advanced basic unit for meshes was designed as shown in Fig. 5D-F. The square basic unit consists of two lugs and two pins on opposing sides. All neighboring units are rotated by 90 °C to connect the lugs and pins and form a stable two-dimensional network. Due to various overhangs in the design, this mesh could only be printed with support structure. After removal of the support structure during thermal debinding and sintering, the mesh was flexible with bending angles of

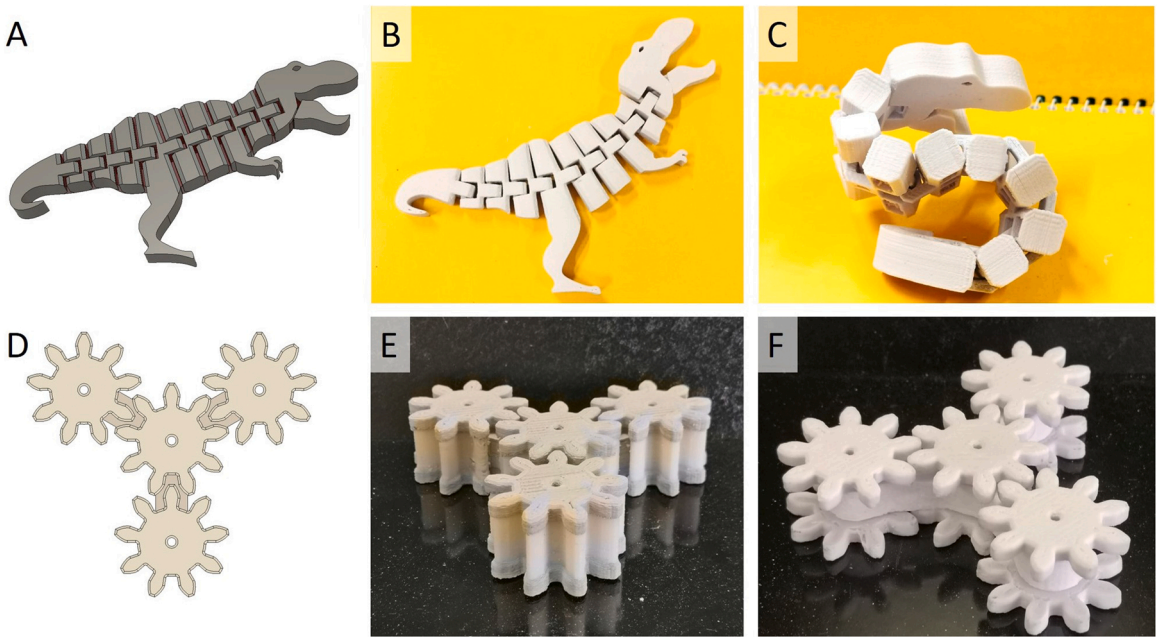

Fig. 6. A: CAD of the T-Rex; B-C: photos of the sintered dinosaur lying on a flat surface and bent. D: CAD of the gearwheel fidget spinner; E: photo of the fidget spinner as printed with NaCl support material; F: sintered fidget spinner.

roughly 10° between the individual links Fig. 5F. This bending angle could be adjusted by varying the vertical spacing between the basic units as well as the horizontal spacing between lugs and pins. Using similar principles, chains with 12–24 links were designed and fabricated in a way that allowed revolving each hinge by 130° (Fig. 5G-J).

Fig. 6 shows two more examples of flexible/movable parts that were printed in one go with Al_2O_3 feedstock and NaCl support material. The dinosaur consists of 10 links connected by hinges with a jaw that can be opened and closed and has a total length of almost 20 cm. The last example is a "fidget spinner"-style toy with a triangular backbone that encloses the shafts of four identical 9-tooth gearwheels. After sintering, all gears are jointly rotatable.

Nowadays, flexible ceramic meshes and chains find their only application in artistic craftwork [16,23], because there are no industrial processes allowing the fabrication of such parts from technical ceramics. However, innovations in different ceramic 3D printing techniques and materials, such as the NaCl support feedstock for ceramic MEX presented herein, could make some applications viable in the future. Opportunities could lie in the jewelry industry (ceramic wristbands for watches, 3D printed bracelets, …) as well as high temperature applications (fully ceramic conveyor belts for continuous furnaces, …) or corrosion and abrasion resistive ceramic gearwheels.

4. Conclusion

A novel support structure material for ceramic MEX printing was demonstrated. The feedstock was based on a commercial CIM binder system, filled with high contents of NaCl (67 vol%). The same binder system was used for the ceramic feedstock and support material, ensuring full compatibility between the two during printing. After dissolving the NaCl in water during pre-debinding of the ceramic part, the remaining support material is burned off during thermal debinding. The binder system as well as NaCl feedstock were characterized using rheology, DSC, TGA and (electron-)microscopy.

The NaCl support material enables the MEX printing of more complex geometries including overhangs and bridges. We were able to 3D print flexible ceramic chains, meshes, hinges and gearwheels from Al_2O_3. By adding this kind of functionality to classical ceramic materials, their range of technical applications can be increased.

With the strategy presented herein, a fully compatible support material for each ceramic or metallic feedstock can be formulated with the same binder but the ceramic or metal powder replaced by NaCl.

Declaration of Competing Interest

The authors declare that they have no known competing financial interests or personal relationships that could have appeared to influence the work reported in this paper.

Acknowledgments

Parts of this work were supported by the Swiss Innovation Agency (Grant no. 55977.1 IP-ENG).

The authors want to thank the many students of Materials and Process Engineering and Mechanical Engineering for their contributions and the colleagues at ZHAW School of Engineering for the support.

Appendix A. Supplementary material

Supplementary data associated with this article can be found in the online version at doi:10.1016/j.jeurceramsoc.2023.03.069.

References

[1] A. Hadian, M. Fricke, A. Liersch, F. Clemens, Material extrusion additive manufacturing of zirconia parts using powder injection molding feedstock compositions, Addit. Manuf. 57 (2022), 102966, https://doi.org/10.1016/j.addma.2022.102966.

[2] R. Wick-Joliat, M. Schroffenegger, D. Penner, Multi-material ceramic material extrusion 3D printing with granulated injection molding feedstocks, Ceram. Int (2022), 118159, https://doi.org/10.1016/j.ceramint.2022.10.170.

[3] D. Nötzel, R. Eickhoff, T. Hanemann, Fused filament fabrication of small ceramic components, Materials 11 (2018) 1463, https://doi.org/10.3390/ma11081463.

[4] N.A. Conzelmann, L. Gorjan, F. Sarraf, L.D. Poulikakos, M.N. Partl, C.R. Müller, F. J. Clemens, Manufacturing complex Al2O3 ceramic structures using consumer-grade fused deposition modelling printers, Rapid Prototyp. J. 26 (2020) 1035–1048, https://doi.org/10.1108/RPJ-05-2019-0133.

[5] M. Orlovská, Z. Chlup, Ľ. Bača, M. Janek, M. Kitzmantel, Fracture and mechanical properties of lightweight alumina ceramics prepared by fused filament fabrication, J. Eur. Ceram. Soc. 40 (2020) 4837–4843, https://doi.org/10.1016/j.jeurceramsoc.2020.02.026.

[6] S. Cano, J. Gonzalez-Gutierrez, J. Sapkota, M. Spoerk, F. Arbeiter, S. Schuschnigg, C. Holzer, C. Kukla, Additive manufacturing of zirconia parts by fused filament fabrication and solvent debinding: selection of binder formulation, Addit. Manuf. 26 (2019) 117–128, https://doi.org/10.1016/j.addma.2019.01.001.
[7] A. Hadian, L. Koch, P. Koberg, F. Sarraf, A. Liersch, T. Sebastian, F. Clemens, Material extrusion based additive manufacturing of large zirconia structures using filaments with ethylene vinyl acetate based binder composition, Addit. Manuf. 47 (2021), 102227, https://doi.org/10.1016/j.addma.2021.102227.
[8] Q. He, J. Jiang, X. Yang, L. Zhang, Z. Zhou, Y. Zhong, Z. Shen, Additive manufacturing of dense zirconia ceramics by fused deposition modeling via screw extrusion, J. Eur. Ceram. Soc. 41 (2021) 1033–1040, https://doi.org/10.1016/j.jeurceramsoc.2020.09.018.
[9] T. Shen, H. Xiong, Z. Li, L. Zhang, K. Zhou, Fused deposition fabrication of high-quality zirconia ceramics using granular feedstock, Ceram. Int. 47 (2021) 34352–34360, https://doi.org/10.1016/j.ceramint.2021.08.348.
[10] L. Gorjan, L. Reiff, A. Liersch, F. Clemens, Ethylene vinyl acetate as a binder for additive manufacturing of tricalcium phosphate bio-ceramics, Ceram. Int. 44 (2018) 15817–15823, https://doi.org/10.1016/j.ceramint.2018.05.260.
[11] J. Schlacher, A.K. Hofer, S. Geier, I. Kraleva, R. Papšík, M. Schwentenwein, R. Bermejo, Additive manufacturing of high-strength alumina through a multi-material approach, Open Ceram. 5 (2021), https://doi.org/10.1016/j.oceram.2021.100082.
[12] S. Weingarten, U. Scheithauer, R. Johne, J. Abel, E. Schwarzer, T. Moritz, A. Michaelis, Multi-material ceramic-based components – additive manufacturing of black-and-white zirconia components by thermoplastic 3D-printing (CerAM - T3DP), J. Vis. Exp. 2019 (2019) 1–10, https://doi.org/10.3791/57538.
[13] V. Lang, S. Weingarten, H. Wiemer, U. Scheithauer, F. Glausch, R. Johne, A. Michaelis, S. Ihlenfeldt, Process data-based knowledge discovery in additive manufacturing of ceramic materials by multi-material jetting (CerAM MMJ), J. Manuf. Mater. Process. 4 (2020), https://doi.org/10.3390/JMMP4030074.
[14] C. Duran, V. Subbian, M.T. Giovanetti, J.R. Simkins, F.R. Beyette Jr, Experimental desktop 3D printing using dual extrusion and water-soluble polyvinyl alcohol, Rapid Prototyp. J. 21 (2015) 528–534, https://doi.org/10.1108/RPJ-09-2014-0117.
[15] Y. Wang, L. Li, D. Hofmann, J.E. Andrade, C. Daraio, Structured fabrics with tunable mechanical properties, Nature 596 (2021) 238–243, https://doi.org/10.1038/s41586-021-03698-7.
[16] Cecil Kempernik, n.d. ⟨https://cecilkemperink.nl/en.html⟩.
[17] N. Kleger, M. Cihova, K. Masania, A.R. Studart, J.F. Löffler, 3D printing of salt as a template for magnesium with structured porosity, Adv. Mater. 31 (2019), https://doi.org/10.1002/adma.201903783.
[18] N. Kleger, S. Fehlmann, S.S. Lee, C. Dénéréaz, M. Cihova, N. Paunović, Y. Bao, J. Leroux, S.J. Ferguson, K. Masania, A.R. Studart, Light-based printing of leachable salt molds for facile shaping of complex structures, Adv. Mater. 34 (2022), 2203878, https://doi.org/10.1002/adma.202203878.
[19] R. Wick-Joliat, M. Tschamper, R. Kontic, D. Penner, Water-soluble sacrificial 3D printed molds for fast prototyping in ceramic injection molding, Addit. Manuf. 48 (2021), 102408, https://doi.org/10.1016/j.addma.2021.102408.
[20] R. Wick-Joliat, S. Mauchle, R. Kontic, S. Ehrat, T. Hocker, D. Penner, MoSi2/Al2O3/Feldspar composites for injection-molded ceramic heating elements, Adv. Eng. Mater. 23 (2021), 2100517, https://doi.org/10.1002/adem.202100517.
[21] H. Warlimont, Ceramics, Springer Handbook of Condensed Matter and Materials Data, Springer Berlin Heidelberg, n.d., pp. 431–476. ⟨https://doi.org/10.1007/3-540-30437-1_6⟩.
[22] A.M. Abyzov, Aluminum oxide and alumina ceramics (review). Part 1. Properties of Al2O3 and commercial production of dispersed Al2O3, Refract. Ind. Ceram. 60 (2019) 24–32, https://doi.org/10.1007/s11148-019-00304-2.
[23] M. Guralnick, Trend alert: ceramic chains as artful decor, Remodelista 10 (2016). ⟨https://www.remodelista.com/posts/trend-alert-ceramic-chains-sculpture/⟩.